Comparison of Wind Speed and Wave Height Trends from Twentieth-Century Models and Satellite Altimeters

ALBERTO MEUCCI AND IAN R. YOUNG

Department of Infrastructure Engineering, University of Melbourne, Parkville, Victoria, Australia

OLE JOHAN AARNES

Norwegian Meteorological Institute, Bergen, Norway

ØYVIND BREIVIK

Norwegian Meteorological Institute, and University of Bergen, Bergen, Norway

(Manuscript received 17 July 2019, in final form 1 October 2019)

ABSTRACT

The trends in marine 10-m wind speed U_{10} and significant wave height H_s found in two century-long reanalyses are compared against a model-only integration. Reanalyses show spurious trends due to the assimilation of an increasing number of observations over time. The comparisons between model and reanalyses show that the areas where the discrepancies in U_{10} and H_s trends are greatest are also the areas where there is a marked increase in assimilated observations. Large differences in the yearly averages call into question the quality of the observations assimilated by the reanalyses, resulting in unreliable U_{10} and H_s trends before the 1950s. Four main regions of the world's oceans are identified where the trends between model and reanalyses deviate strongly. These are the North Atlantic, the North Pacific, the Tasman Sea, and the western South Atlantic. The trends at +24-h lead time are markedly weaker and less correlated with the observation count. A 1985–2010 comparison with an extensive dataset of calibrated satellite altimeters shows contrasting results in H_s trends but similar U_{10} spatial trend distributions, with general agreement between model, reanalyses, and satellite altimeters on a broad increase in wind speed over the Southern Hemisphere.

1. Introduction

Long-term changes in ocean surface wind speed and wave height have received increasing attention as climate change impacts have become evident (Young et al. 2011; Mentaschi et al. 2018; Luijendijk et al. 2018; Young and Ribal 2019). Changes in surface wind speed and wave height may dramatically affect coastal communities (Ranasinghe 2016), as well as offshore operations (Bitner-Gregersen et al. 2018), but uncertainties still characterize our current knowledge of long-term variations in these quantities (Rhein et al. 2013).

Trend analyses of global ocean surface wind speed and wave height rely on observational and modeled datasets. Long time series of surface wind speed and wave height observations originate from shipboard measurements that date back to 1854, the year marking the beginning of an internationally organized system for recording shipboard meteorological observations (Maury 1853; Cardone et al. 1990; Woodruff et al. 1998). These datasets are mainly derived from Voluntary Observing Ships (VOS). Studies of VOS marine wind speed have shown that these datasets are affected by changes in measuring techniques. This is especially relevant in the first part of the century, where the absence of universal standards for estimated winds (formalization of sea-state equivalent Beaufort scale took place in 1946; Thomas et al. 2008) may have permanently compromised trend studies of ocean surface wind speed over this period (Peterson and Hasse 1987; Ramage 1987). These findings were confirmed by Cardone et al. (1990) who voiced general skepticism on the possibility of

Denotes content that is immediately available upon publication as open access.

Corresponding author: Alberto Meucci, ameucci@student.unimelb.edu.au

DOI: 10.1175/JCLI-D-19-0540.1

removing the spurious trends caused by the presence of inhomogeneities before 1950. After 1950, VOS wind observations show an increasing trend in some areas of the oceans due to a growing number of observations as well as changes in anemometer heights, instrument calibration, and ship size (Cardone et al. 1990). After bias correcting the VOS wind datasets, an increasing signal still remains in the surface wind speed (Thomas et al. 2008; Tokinaga and Xie 2011), leaving open questions as to whether these residual trends are real or affected by other artificial factors (Tokinaga and Xie 2011).

VOS wave height observations are less affected by changes in measurement approaches. However, the coding system had several changes, with the most significant happening in 1950 (Kent et al. 2019). An extensive analysis of VOS wave height time series (Gulev and Grigorieva 2004) found increasing trends in the Atlantic from 1950 to 2002, but no significant trends on the total 1885–2002 period, again questioning the quality of the measurements in the first part of the twentieth century. Increasing trends in the Pacific (1950–2002) were found to be considerably weaker compared to the North Atlantic region (Gulev and Grigorieva 2004). However, the analysis was limited to the main ship routes, with limited coverage in the Southern Hemisphere.

Buoy measurements started in the 1970s and cover only a small area of the oceans. Trends in wind speed and wave height have been investigated from buoy measurements in some areas of the oceans such as the northeast Pacific (Allan and Komar 2000; Gower 2002; Ruggiero et al. 2010) and the Southern Ocean (Hemer 2010). However, these trend analyses may also be affected by spurious effects and step changes in the records due to changes in instrumentation, buoy hulls, and measurement techniques (Gemmrich et al. 2011; Thomas and Swail 2011).

The advent of ocean-observing satellites in the late 1970s represents a fundamental step forward in the understanding of marine wind and wave climate. These datasets guarantee global coverage of the ocean, drastically increasing the amount of observations in previously poorly observed areas such as the Southern Ocean. Today these datasets constitute time series covering a period of over 30 years (Young et al. 2011; Young and Ribal 2019).

However, for trend analysis even longer datasets are desired. This would reduce the effect of natural variability (Dobrynin et al. 2015; Kumar et al. 2016) and help identify potential climate change signals (Weisse 2010).

Reanalyses and hindcasts (without assimilation) have been widely used for both weather and climate applications at both regional and global scales (Gregow et al. 2016), as they represent the best available interpolated datasets in space and time. Trend studies have also taken advantage of reanalyses' long and spatially homogeneous time series that cover the whole globe (Semedo et al. 2011; Bertin et al. 2013; Wang et al. 2012, 2013; Aarnes et al. 2015). The European Centre for Medium-Range Weather Forecasts (ECMWF) and the National Oceanic and Atmospheric Administration (NOAA) have recently extended reanalyses back to the beginning of the twentieth century (Compo et al. 2011; Poli et al. 2016; Laloyaux et al. 2018). These datasets are interesting candidates for investigation of long-term wind and wave climate. However, changes caused by increasing numbers of assimilated observations throughout the years, may produce spurious trends (Bengtsson et al. 2004; Weisse 2010; Aarnes et al. 2015; Wohland et al. 2019). Inconsistent surface wind speed trends have been found between the ECMWF century-long reanalyses (ERA-20C and CERA-20C) and the twentieth-century NOAA climate reanalysis (20CR) (Compo et al. 2011). Considering the North Atlantic and North Pacific, Wohland et al. (2019) argue that spurious trends might be connected to the growing number of marine wind speed observations assimilated by the ECMWF reanalyses. Furthermore, the ERA-20C (Poli et al. 2016) and the NOAA 20CR were found to be inconsistent in the low-frequency variability of the Northern Hemisphere winter seasons (Befort et al. 2016).

So far, no studies have been carried out on wave height long-term trends of these reanalysis products. Waves are a combination of local wind-sea and swell coming from distant storms (Young 1999b). Despite being entirely forced by the wind field, the long-term trends of wave height may be affected by low-frequency variability, for example, increasing number of cyclones, in the form of a swell contribution (Young 1999a; Gulev and Grigorieva 2006). This is also found in climate projections, where significant changes in extratropical swell can be found toward the end of the twenty-first century (Shimura et al. 2016; Breivik et al. 2019).

This work aims to investigate the relevance of trend analysis of 10-m surface wind speed, and significant wave height, obtained from the ERA-20C (Poli et al. 2016) and CERA-20C (Laloyaux et al. 2018) and compare with the ERA-20CM (Hersbach et al. 2015a) atmosphere–wave model-only integration (i.e., without assimilation). To further investigate the relevance of U_{10} and H_s trends from twentieth-century climate models and reanalyses, we compare the ECMWF century-long datasets, with and without assimilation of in situ observations, with the trends of an independent dataset of calibrated satellite altimeter observations (Ribal and Young 2019; Young and Ribal 2019). The objective is to investigate twentieth-century U_{10} and H_s long-term changes and to evaluate the relevance of climate studies derived from twentieth-century models. Furthermore, data assimilation impacts will be assessed by comparing with trends at +24-h forecast lead

TABLE 1. Characteristics of the ECMWF century-long models.

	ERA-20CM	ERA-20C	CERA-20C
Ensemble members	10	1	10
Assimilation atmosphere	Model-only integration	Marine wind, surface pressure	Marine wind, surface pressure
Atmosphere–waves–land	Coupled	Coupled	Coupled
Coupled ocean–ice	Prescribed HadISST2.1.0.0	Prescribed HadISST2.1.0.0	Coupled
Assimilation ocean	—	—	Temperature, salinity
Radiative forcing	CMIP5	CMIP5	CMIP5
Horizontal resolution	Atmosphere: 125 km Ocean: 166 km	Atmosphere: 125 km Ocean: 166 km	Atmosphere: 125 km Ocean: 110 km
IFS	cy38r1 (2012)	cy38r1 (2012)	cy41r1 (2015)
OFA	—	Public	Public

time (Aarnes et al. 2015). This analysis provides a mechanism to determine the level of confidence in the climate change signal in ocean wind speed and significant wave height over the twentieth century.

The paper is structured as follows. Section 2 describes the datasets used for the trend analysis and explains the approach used to calculate trend magnitude and statistical significance. Section 3 describes the century-long trends. Section 4 analyses the differences between each model representation of climate averages over the twentieth century. Section 5 concentrates on comparing the climate model and reanalysis trends with the satellite altimeters trends. Sections 6 and 7 discuss the possibility of a real climate signal and our confidence in the estimated trends. Finally, we include our recommendations on how to interpret trends from reanalyses.

2. Datasets and methodology

ECMWF (Dee et al. 2014; Buizza et al. 2018) and NOAA (Compo et al. 2011) have recently developed state-of-the-art reanalyses that cover the whole twentieth century. The aim is to obtain a better understanding of the past to improve current weather forecasts and climate studies (Buizza et al. 2018). ECMWF developed three different century-long datasets: (i) ERA-20CM (Hersbach et al. 2015a), (ii) ERA-20C (Poli et al. 2016), and (iii) CERA-20C (Laloyaux et al. 2018). Table 1 describes the characteristics of the three models.

ERA-20C and CERA-20C are interesting in the context of trend analysis because in contrast with ERA-20CM, which is a model-only integration, they assimilate in situ observations of surface pressure and marine surface winds. Neither reanalysis assimilates satellite or in situ ocean wave height measurements. This allows us to compare their trends with independent satellite altimeter wave height measurements. The atmosphere horizontal resolution of the three model integrations is 125 km, whereas the ocean model resolution is 166 km for ERA-20CM and ERA-20C and 110 km for CERA-20C. The models employ the same CMIP5 radiative forcing scheme. The 10-m surface wind speed U_{10} and significant wave height H_s are available as monthly averages of daily means, or as monthly averages of daily outputs at specific synoptic times. The latter have been selected for the trend analysis of the period from 1901 to 2010, and to perform a comparison with independent satellite altimeter trends for the overlapping 1985–2010 period. The main characteristics of each dataset used in this study are described in the following paragraphs in the context of trend analysis.

a. ERA-20CM

ERA-20CM (Hersbach et al. 2015a) is a 10-member ensemble model-only simulation that covers the period 1899–2010. The model version is the Integrated Forecasting System (IFS) cycle 38r1 (released in 2012, see https://bit.ly/2OXuHFF). No observations are assimilated in ERA-20CM, and thus the model is not able to accurately reproduce actual synoptic states. Despite this, ECMWF argues that the ERA-20CM model still performs well in terms of long-term climate, being consistent with other CMIP5 models. As noted also by Dee et al. (2014) the models require boundary conditions that are implemented from other models that in turn depend on observations from multiple sources. ERA-20CM boundary conditions include sea surface temperature (SST) and sea ice states from the Hadley Centre Global Sea Ice and Sea Surface Temperature dataset, version 2 (HadISST2), model (Rayner et al. 2006), developed as part of the same ERA-CLIM European project.

b. ERA-20C

ERA-20C (Poli et al. 2016) is a single-member reanalysis for the period 1900–2010. It assimilates in situ observations of surface pressure from the International Surface Pressure Databank (ISPD), version 2 (Cram et al. 2015), and both marine surface pressure and surface wind speed from the International Comprehensive Ocean–Atmosphere Dataset (ICOADS), version 2.5 (Woodruff et al. 2011). The model has the same atmospheric general circulation configuration

as the control member of ERA-20CM and employs the same model version. Surface boundary conditions are also provided by HadISST. This allows for a direct comparison of the trend analysis between the two models. In well-sampled regions, the assimilation of observations adds precision at the synoptic scale, however, a negative impact has been observed on trends and low-frequency variability (Poli et al. 2016). Two main aspects of the model integrations will be investigated: the observational constraints and the realism of long-term trends.

c. CERA-20C

CERA-20C is the first atmosphere–ocean coupled climate reanalysis of the twentieth century (Buizza et al. 2018). It is a 10-member ensemble and covers the period from 1901 to 2010 (Laloyaux et al. 2018). It is based on the CERA coupled data assimilation system (Laloyaux et al. 2016) and employs IFS cycle 41r1 of 2015. Like ERA-20C, it assimilates surface pressure and marine wind observations. In addition, it assimilates ocean temperature and salinity profiles. Coupled models have been shown to be crucial for synoptic weather representations. They are especially relevant in the prediction of tropical cyclones (Mogensen et al. 2017), and for a consistent global transport of mass, water, and energy at the relevant time scales (Dee et al. 2014). Despite these models being potentially the best available to reconstruct Earth's climate system and thus wind and wave conditions, open questions remain as to the impact of data assimilation on long-term trends and how these compare to ERA-20CM and ERA-20C.

All models described are coupled to the same version of the ECMWF global third-generation wave model (WAM; WAMDI Group 1988; Janssen 2004), which resolves the two-dimensional wave spectrum, taking into account advection, wind input, bottom friction, nonlinear interactions, and dissipation due to white capping. At each time step the wave model interacts with the atmosphere as surface roughness is fed back to the atmospheric boundary layer scheme of IFS.

d. Observation Feedback Archive

ECMWF produces an Observation Feedback Archive (OFA) (Dee et al. 2014) where all observations used in the data assimilation are archived with the corresponding model values interpolated to the observation location (Hersbach et al. 2015b). Here we investigate the feedback archive of ICOADS v2.5 (Woodruff et al. 2011) surface pressure and wind speed and ISPD v2.2 (Cram et al. 2015) surface pressure.

1) ICOADS v2.5

ICOADS is regarded as the reference long-term marine surface dataset (Woodruff et al. 2011). The ICOADS monthly summary statistics have been produced at a $2° \times 2°$ resolution covering the period 1800–1960 and at $1° \times 1°$ resolution since 1960. There are eight observed variables: SST, air temperature, wind speed, wind components, sea level pressure (SLP), total cloudiness, and relative humidity. There are also 14 derived variables. No attempt is made to account for observing system changes and measurement biases (Woodruff et al. 2011). Critical metadata such as instrument type and placement are used to improve accuracy. However, effects of changes in measurement techniques and the growing number of observations may still affect estimates of long-term trends in the dataset. In Table 2 the surface pressure and wind speed observation counts are listed by measurement technique. These are the observations that have been assimilated in the ERA-20C and CERA-20C.

Figure 1 shows the yearly counts classified by report type over the complete duration of the reanalysis. The vast majority of observations assimilated by ECMWF reanalyses were collected from ships, that is, report type 16008. As shown in Fig. 1, ship measurements started to decrease in the last part of the twentieth century, and observation of the oceans now heavily relies on satellites and drifting buoys (Kent et al. 2006). The observation counts derived from the OFA are crucial to determining the main drivers of trend differences between models and reanalyses (Wohland et al. 2019).

2) ISPD v2.2

The ISPD is the world's largest surface and sea level pressure dataset. The dataset consists of observations from land stations, marine observations and tropical cyclone best track reports (Cram et al. 2015). This dataset was first used in the NOAA twentieth-century reanalysis 20CR and then also assimilated by ERA-20C and CERA-20C.

Figure 2 compares global observation counts of the three observational datasets considered here (ICOADS v2.5 surface wind, ICOADS v2.5 surface pressure, and ISPD v2.2 surface pressure). The counts are binned on a $2° \times 2°$ grid. The comparison shows how the majority of ocean in situ observations have been collected in the Northern Hemisphere with some isolated areas in the Southern Hemisphere such as the Tasman Sea, between Australia and New Zealand, and the South Atlantic ship routes that connect South American and African coasts to the Northern Hemisphere. Figures 2a and 2b clearly show the main ocean ship routes. In the ICOADS wind speed observations plot (Fig. 2a) the tropical ocean mooring buoy array can be clearly observed. Figure 2c shows the ISPD surface pressure observation density, mainly composed of land observations with localized areas of ocean observations. Considering the distribution of the observation density shown in Fig. 2, we focus

TABLE 2. ICOADS 2.5 dataset. Surface pressure and wind speed observation counts (obs) classified by report type ID, as archived in the OFA of the ECMWF (Hersbach et al. 2015b).

ID	Description	No. of pressure obs	No. of wind obs
16005	Drifting and mooring buoys	—	845 712
16008	Ship	5 593 209	4 845 002
16049	Ocean station vessel on station	81 830	120 308
16050	Ocean station vessel off station	32 842	55 488
16051	Station or ship on ice	17 022	7944
16052	Ocean bottle and low-resolution conductivity temperature depth (CTD and XCTD)	—	21 734
16053	Mechanical or digital or microbathythermograph (MBT)	—	33 062
16054	Expendable bathythermograph (XBT)	—	4496
16055	Coastal-marine automated network (CMAN)	289 524	12 384
16056	Undulating oceanographic recorder (UOR)	7	380
16057	Fixed ocean platform or rig	20 211	12 256
16061	High-resolution conductivity temperature depth (CTD and XCTD)	—	812

on the ICOADS dataset to investigate the data assimilation impact on the model climate trends.

e. *Satellite altimeters*

To further assess long-term climate performance of the ECMWF reanalyses and model-only integrations, we compare the trends of the last part of the century-long model runs with the trends found from the largest available dataset of satellite measurements of U_{10} and H_s (Young and Ribal 2019). This archive is calibrated and cross validated against buoys from the U.S. National Data Buoy Center (NDBC) and independent buoy datasets (Ribal and Young 2019). The calibrated satellite altimeter observations span the period 1985–2018. To compare with the ECMWF model integrations, we analyze the overlapping 1985–2010 window, noting that before 1991 the amount of altimeter data is relatively sparse, as only one satellite was operational. The horizontal resolution of this satellite altimeter dataset is 2° × 2°. The comparison is particularly interesting given the fact that the ECMWF century-long model integrations do not assimilate satellite observations to avoid impact of sudden changes in the assimilated observations (Weisse 2010; Sasaki 2016).

f. *Trend analysis*

To perform the trend analysis we select the monthly mean H_s and U_{10} values from the three ECMWF century-long models and the satellite altimeter observations. We apply a nonparametric trend analysis using

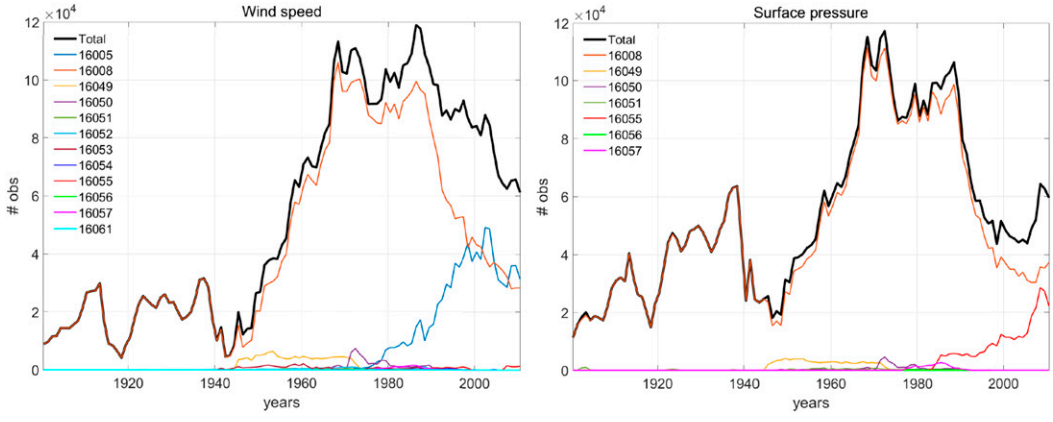

FIG. 1. The 1901–2010 ICOADS 2.5 (left) surface wind and (right) surface pressure observation yearly counts divided by report type, as archived in the ECMWF Observational Feedback Archive. Refer to Table 2 for the description of report type ID.

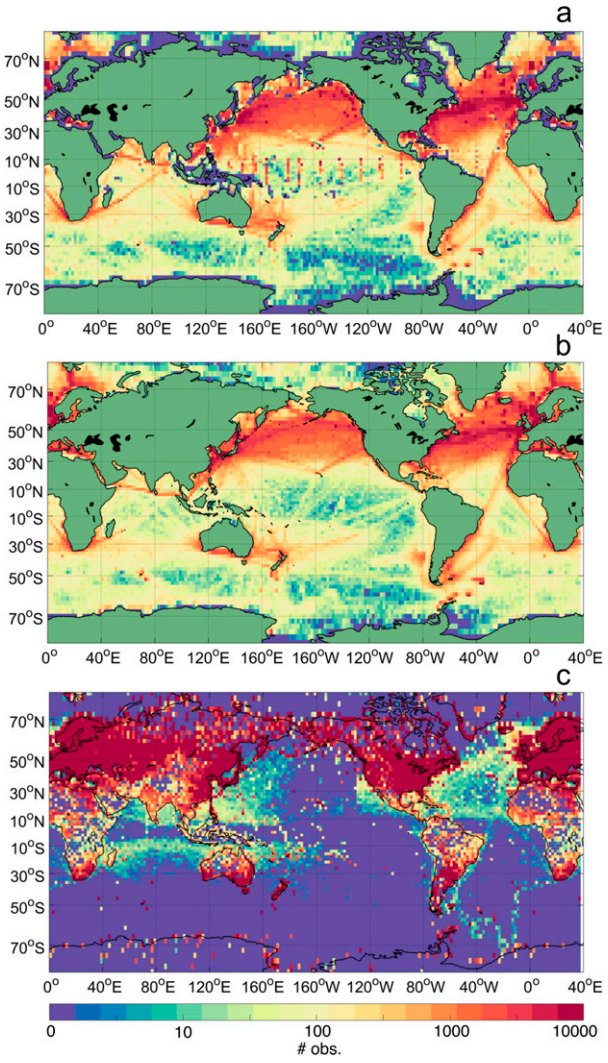

FIG. 2. The 1901–2010 OFA observations counts in a base-10 logarithmic scale, binned on a 2° × 2° grid. The three different datasets assimilated in ERA-20C and CERA-20C are (a) ICOADS2.5 surface wind, (b) ICOADS2.5 surface pressure, and (c) ISPD2.2 surface pressure.

the Theil–Sen estimator (Theil 1950; Sen 1968). Compared to a regression analysis, this method is more robust for nonnormally distributed data, such as in the case of H_s, and has the advantage of reducing the impact of potential outliers. The approach has previously been used to estimate trends of marine wind speed and significant wave height from model reanalyses (Wang and Swail 2001; Aarnes et al. 2015) and from satellite observations (Young et al. 2011; Young and Ribal 2019). The trend magnitude is found by selecting the median of the slopes (change per unit of time) computed for each month, between distinct pairs (i, j) of monthly mean values, as shown by

$$\text{median}\left(\frac{X_j - X_i}{t_j - t_i}\right), \quad 1 \le i \le j \le n, \quad \text{with } i \ne j, \qquad (1)$$

where n is the number of years, and X takes, respectively, the monthly mean values of H_s or U_{10}. The Sen's slope is computed for each month, and $t_j - t_i$ is the difference in time (years). The trend at each location of the globe is the median of the monthly slopes. To evaluate the significance of the trend at each gridpoint location, we perform a Mann–Kendall test (Mann 1945; Kendall 1948) adapted to account for seasonality and serial dependence (Hirsch et al. 1982; Hirsch and Slack 1984). To test the serial dependence of monthly mean H_s and U_{10}, we computed the Pearson correlation between consecutive months (monthly lag-1 correlation) for the three ECMWF models considered in this study. The results show that two consecutive monthly mean values are globally correlated with a Pearson coefficient generally higher than 0.4. This is the case for both H_s and U_{10} monthly means from the three ECMWF models. Thus, serial dependence is accounted for in the seasonal Mann–Kendall trend test (SKTT) with the covariance term introduced by Dietz and Killeen (1981).

3. Century-long trends

The H_s and U_{10} 1901–2010 trends from the three ECMWF twentieth-century models are shown in Fig. 3 as percentage change per decade. Only the trends with 95% significance from the SKTT are shown. The ensemble model trends are found for the 10-member ensemble mean. Figure 3 shows that the ERA-20C and CERA-20C trends differ significantly from the ERA-20CM model trends. Two areas stand out with a significant positive trend in the ERA-20CM: the Southern Ocean high latitudes (5–10 cm s^{-1} $decade^{-1}$ change in U_{10}; 1–2 cm $decade^{-1}$ change in H_s) where the different sea ice cover derived from the model boundary condition may play a role (Fig. 3b), and the western tropical Pacific (3–7 cm s^{-1} $decade^{-1}$ for U_{10}; no significant trend in the H_s), where the strong recent La Niña episode affects the trend of the entire century (de Boisséson et al. 2014). The trend in the Southern Ocean could be correlated to the different surface roughness related to the changes in sea ice cover found by the SST/sea ice conditions of HadISST2 (Rayner et al. 2006). The H_s domain is masked at the latitudes of sea ice cover (hatched regions in Fig. 3a). The H_s trends are spatially uniform compared to the U_{10} trends. A slight decrease in H_s (≈ -0.5 cm $decade^{-1}$) is depicted at midlatitudes with the exception of the South Atlantic region. In contrast, the deterministic reanalysis, ERA-20C, shows mostly increasing trends with magnitudes in the Northern Hemisphere that exceed +1.75% $decade^{-1}$ (up to

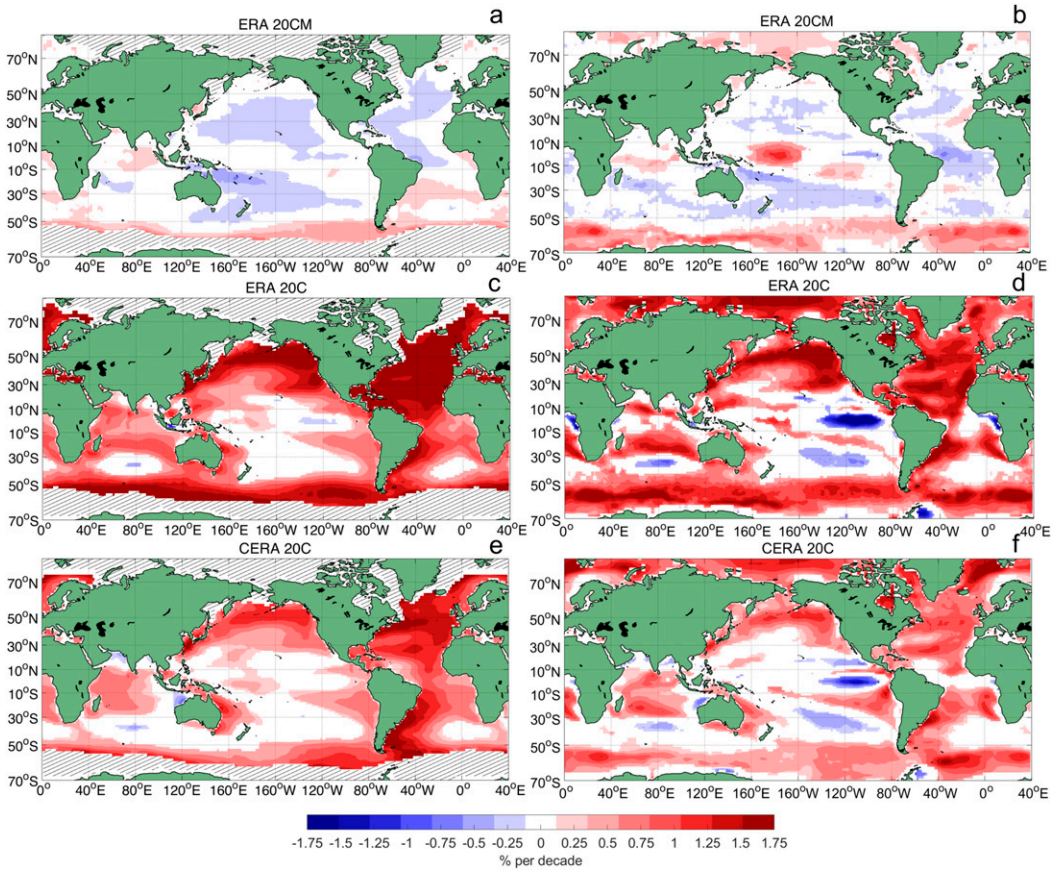

FIG. 3. The 1901–2010 trends (% decade^{-1}). Comparison between the three twentieth-century ECMWF datasets—(a),(b) ERA-20CM, (c),(d) ERA-20C, and (e),(f) CERA-20C—for (left) H_s and (right) U_{10}. Only the 95% significant trends from the SKTT are plotted. White regions represent areas where the trend is not statistically significant. Sea ice cover areas that limit the H_s domain are hatched.

18 cm s^{-1} decade^{-1} change in U_{10} and 5–8 cm decade^{-1} change in H_s). The CERA-20C spatial trend distribution is very similar to the ERA-20C results, but with reduced magnitude (up to 8 cm s^{-1} decade^{-1} change in U_{10} and up to 5 cm decade^{-1} change in H_s). This could be related to the 10-member ensemble averaging process or to the dampening effect of the coupled ocean model caused by the assimilation of subsurface ocean measurements (Wohland et al. 2019). A significant increase in both H_s and U_{10} is found, especially in the Northern Hemisphere, for both ERA-20C and CERA-20C. The spatial distribution of the strongest trends found in these reanalyses is remarkably similar to the spatial distribution of the areas with the highest observation counts, as shown in Fig. 2. This is particularly true for the ICOADS dataset (Figs. 2a,b) and in agreement with the analysis by Wohland et al. (2019). Given the similarities between ERA-20C and CERA-20C trends, and assuming that the ensemble approach is more reliable in finding relevant trends, we concentrate our further investigations only on the comparison between the two ensemble models (ERA-20CM and CERA-20C).

+24-h forecast lead-time trends

To assess to what extent the differences in the CERA-20C trends are related to the assimilated observations, and how this is sustained through the model forecast time, we performed a trend analysis at the +24-h forecast lead time (FC24). Note that the +24-h lead time is the only forecast dataset available online for these models. Aarnes et al. (2015) used the +48-h forecast lead time to lessen the impact of data assimilation on the ERA-Interim trends. The percentage-per-decade trend difference between CERA-20C at analysis time (ANA) and +24-h forecast lead time (FC24) is shown in Fig. 4 (ANA-FC24). The trend in the analysis is larger than the forecast (positive values in Fig. 4), especially in the areas where the main differences in the number of observations are found, that is, in the Northern Hemisphere and in localized areas of the Southern Hemisphere (Figs. 2a,b). The

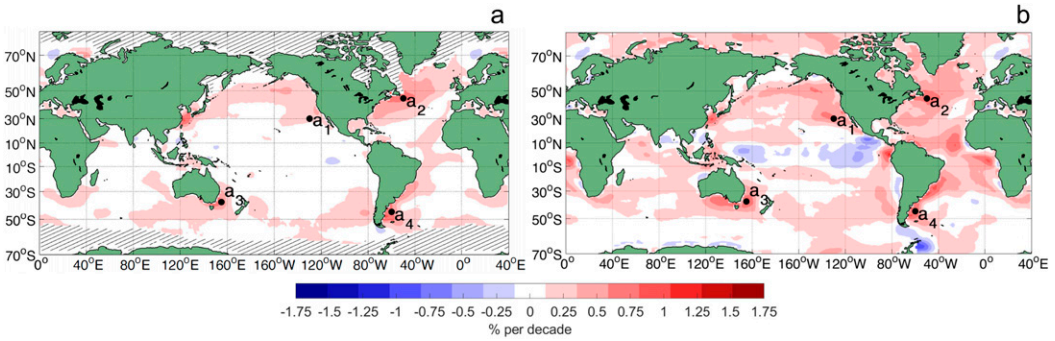

FIG. 4. Difference in CERA-20C 1901–2010 trends (% decade^{-1}) between analysis time (ANA) and forecast lead time +24 h (FC24) for (a) H_s and (b) U_{10}. Sea ice cover areas that limit the H_s domain are hatched.

differences are larger for U_{10} (Fig. 4b), because the wind speed is a parameter directly assimilated from the ICOADS2.5 dataset, whereas H_s is a derived variable (Fig. 4a). Again, the H_s spatial variability is more uniform compared to the wind speed due to the different nature of these two variables. Differences between ANA and FC24 H_s are less pronounced, showing a smaller impact of data assimilation on H_s climate, but remarkably similar to the ICOADS pattern in Fig. 2a.

To further investigate the areas where the observational datasets significantly impact the century-long trends, we select four locations with the largest differences between ANA and FC24 trends. The locations are shown in Fig. 4b. At these locations we compute the yearly averages for all three models. Figure 5 shows the yearly average values of U_{10} and H_s for the reanalyses ERA-20C and CERA-20C (green and red lines) and the model-only integration ERA-20CM (blue lines) at ANA and FC24. Large differences are found in the first part of the century. At location a_1 the reanalyses show a change in the trend direction across the century, with an unusual decrease in the first part of the twentieth century. Again, the comparison between ANA and FC24 confirms that the data assimilation effect is reduced in the forecast case of U_{10} but not significantly for H_s. The FC24 ensemble spread is larger than the ANA spread as expected. Location a_3 in the Tasman Sea shows a significant reduction in the average difference between the two reanalyses and ERA-20CM at FC24 compared to ANA. Figure 5 generally reveals large differences in the first part of the twentieth century. This difference is also present for H_s at FC24. However, the U_{10} ANA yearly average difference between models is significantly reduced at FC24.

4. Twentieth-century climate

We compare the H_s and U_{10} yearly averages and investigate the differences between the ERA-20CM model and CERA-20C climate at the global scale. The normalized difference in the yearly averages is found using

$$d = \frac{\overline{x}^{\,\mathrm{ERA20CM}} - \overline{x}^{\,\mathrm{CERA20C}}}{\overline{x}^{\,\mathrm{ERA20CM}}}, \tag{2}$$

where $\overline{x}$ is the yearly average, respectively, of H_s or U_{10} monthly means. The differences are normalized over the ERA-20CM yearly averages to obtain a percentage difference. The results are shown in Fig. 6 for three different time periods: 1901–2010 (Figs. 6a,b), 1901–30 (Figs. 6c,d), and 1985–2010 (Figs. 6e,f). It is interesting to note that the yearly average H_s differences between the two models are generally higher than the U_{10} differences, showing that the impact of data assimilation of U_{10} and SLP have a marked effect on wave climate. In the first part of the century, 1901–30 (Figs. 6c,d), the climate differences are larger, whereas the last part of the century, 1985–2010 (Figs. 6e,f), shows a better agreement between the models. This is consistent with the location analysis performed in Fig. 5. The ERA-20CM climate is consistently higher for both H_s and U_{10} yearly averages throughout the century. Some areas show closer agreement, such as the 30°–40°N latitude band in the western North Pacific, where we find significantly smaller differences between the models than other regions. Initially, this singular pattern of similarity might be attributed to the average ship routes that follows higher latitudes on the great circle between Asia and North America. However, a more detailed analysis of observation counts shows that also at these latitudes the number of observations increases throughout the dataset time period. Given that ERA-20CM and CERA-20C both have SST boundary conditions dictated by the HadISST2 model, these similarities could be related to SST-induced winds. This area is indeed impacted by the Kuroshio Extension phenomenon, characterized by strong seasonal variations of SST temperature that affect surface winds (Nonaka and Xie 2003). These findings, if confirmed, could further

FIG. 5. Yearly averages of monthly mean values at four different locations indicated in Fig. 4b. For ERA-20CM and CERA-20C, the envelope of the ensemble values are plotted together with the mean. Columns represent (left to right) ANA H_s, FC24 H_s, ANA U_{10}, and FC24 U_{10}, respectively.

demonstrate the impact of SST boundary conditions on modeled ocean surface climate. In general, H_s and U_{10} yearly average differences show similar spatial distribution. For the complete 1901–2010 dataset, the absolute H_s differences are between −0.15 and 0.5 m, whereas, the U_{10} differences are between −1.8 and 2 m s^{-1}. The H_s and U_{10} maximum absolute differences are found at the high latitudes. Larger discrepancies between ERA-20CM and CERA-20C are found again in the areas with most assimilated observation from the ICOADS dataset (Figs. 2a,b).

5. Model, reanalysis, and satellite trends

Considering the large difference in H_s and U_{10} climate representation in the first part of the century, and to further investigate the ECMWF dataset performance in long-term climate analyses, we here compare the 1985–2010 model and reanalysis trends with trends calculated from calibrated satellite altimeter dataset (Young and Ribal 2019; Ribal and Young 2019). The trends are shown in Fig. 7 in terms of percentage change per decade. The dotted areas are regions where the trends are significant at the SKTT 95% level. Few locations show a statistically significant trend in H_s for both the satellite altimeter (Fig. 7a) and ERA-20CM (Fig. 7c), demonstrating general agreement between the datasets. In contrast, the altimeter U_{10} trends (Fig. 7b) are largely significant in the Southern Hemisphere, whereas the ERA-20CM U_{10} trends (Fig. 7d), show only few statistically significant areas of the oceans with lower trend magnitudes. Different U_{10} trends are also found in the northeast Pacific. Here, the altimeters depict an increasing trend that is in contrast with the decreasing values found in ERA-20CM. However, the results do show similar spatial distribution for both H_s and U_{10} between the satellite altimeter and ERA-20CM

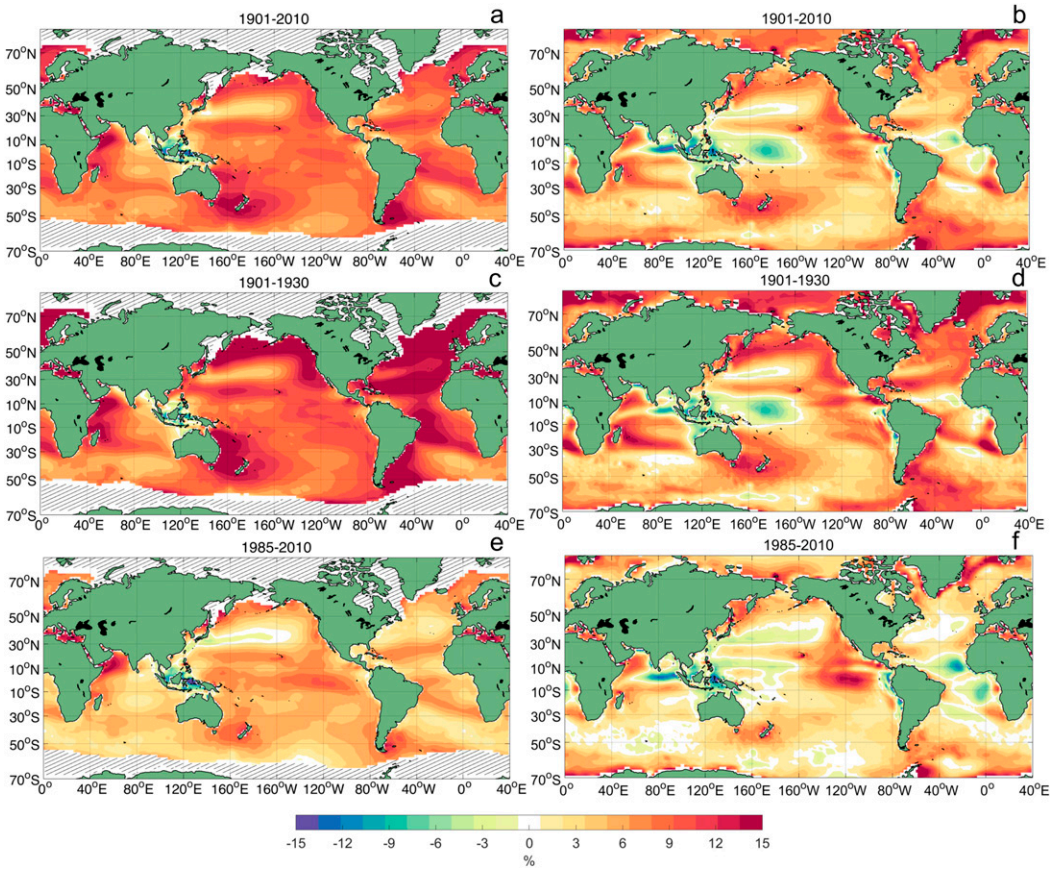

FIG. 6. Annual averages of monthly mean values. Differences between ERA-20CM and CERA-20C [Eq. (2)] are shown for (left) H_s and (right) U_{10} for the periods of (a),(b) 1901–2010, (c),(d) 1901–30, and (e),(f) 1985–2010. Sea ice cover areas that limit the H_s domain are hatched.

results. For instance, the U_{10} altimeter and ERA-20CM trends (Figs. 7b,d) both show a significant increase in the central Pacific (de Boisséson et al. 2014), a positive band across the tropical Atlantic, and a general increase across the Southern Ocean. Also, both figures show an increase in the central Indian Ocean and a reduction in the southern Indian Ocean (agreement less clear). Also, the H_s altimeter and ERA-20CM trends (Figs. 7a,c), show a small increase in the Southern Ocean west of South America, the increase in the central Pacific already noted for U_{10}, a decrease in the North Pacific, and a slight increase in the Atlantic east of the Gulf of Mexico.

A greater spatial difference in distribution is found between the altimeter trends (Figs. 7a,b) and the CERA-20C trends at analysis time (Figs. 7e,f). Compared to both satellite and ERA-20CM results, the CERA-20C H_s trends (Fig. 7e) show larger differences than the U_{10} trends. CERA-20C results show a generally increasing U_{10} trend in the Southern Hemisphere (Fig. 7f) that is further amplified in the H_s trends (Fig. 7e). The reason for the large trends in the H_s coupled CERA-20C in the Southern Hemisphere is not clear. We speculate that the large positive trends in Southern Hemisphere midlatitudes (Fig. 7e) may be associated with an increase of swell propagating from the Southern Ocean. However, this possibility requires further analysis of, for instance, changes in wave period.

Although there are differences in magnitude, all three datasets compared here show increasing U_{10} in the Southern Hemisphere, with similar spatial distribution. The analysis of the CERA-20C FC24 trends (not shown here) does not differ significantly from the results obtained at ANA shown in Figs. 7e and 7f. This means that data assimilation for the period 1985–2010 is not affecting U_{10} trends as strongly as is the case when the whole twentieth century is considered.

6. Discussion

The present work found generally inconsistent twentieth-century H_s and U_{10} trends for an ECMWF model-only integration (ERA-20CM) and reanalyses (ERA-20C and

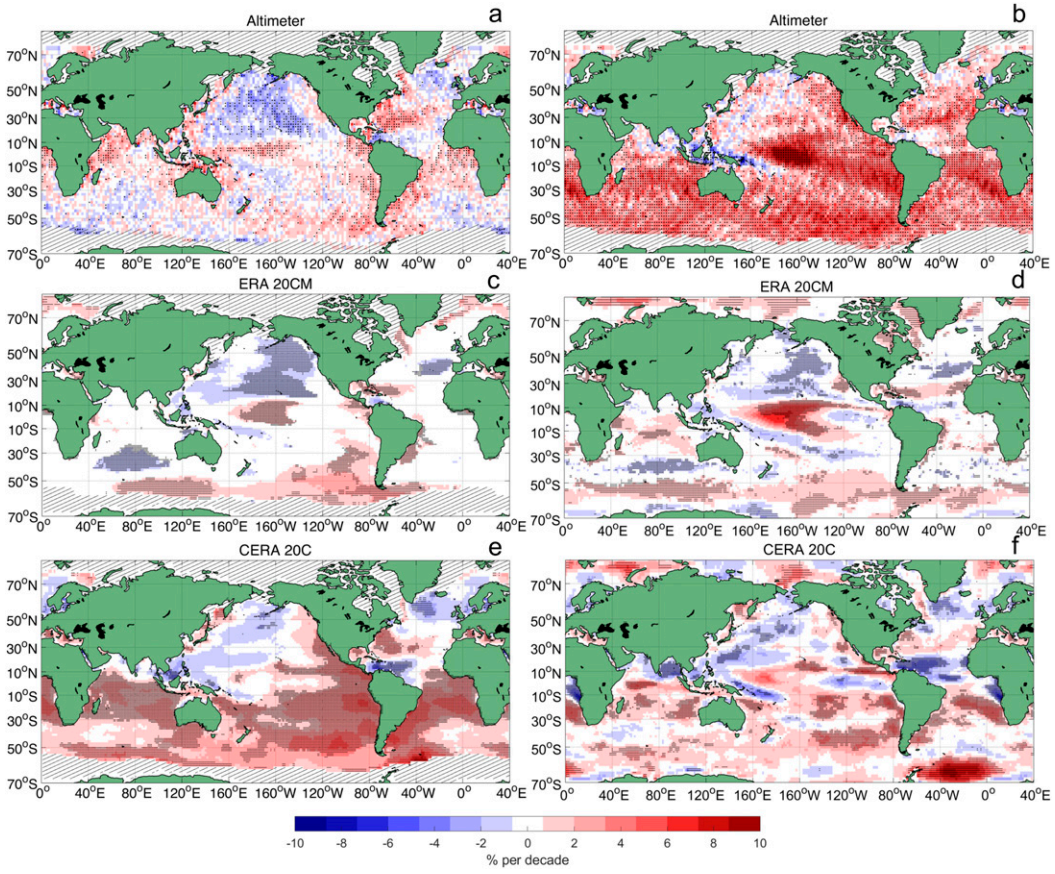

FIG. 7. The 1985–2010 trends (% decade^{-1}). Comparison between (top) altimeter dataset trends (2° × 2°) (Young and Ribal 2019; Ribal and Young 2019), (middle) ERA-20CM, and (bottom) CERA-20C at analysis time (1.5° × 1.5°) for (a),(c),(e) H_s trends and (b),(d),(f) U_{10} trends. Areas of SKTT 95% statistical significance level are dotted. Sea ice cover areas are hatched.

CERA-20C). This is also in agreement with previous studies that compared the ECMWF reanalysis datasets with the NOAA twentieth-century reanalysis (20CR) (Befort et al. 2016; Wohland et al. 2019). NOAA 20CR assimilates ISPD surface pressure measurements but does not show any inconsistencies in trends compared with ECMWF's model-only integration, ERA-20CM (Compo et al. 2006, 2011; Befort et al. 2016; Wohland et al. 2019). This suggests that the main impact on trends might be caused by the ICOADS dataset assimilation in the ECMWF reanalyses. It is not clear if the assimilated ISPD surface pressure measurements (Fig. 2c) also have a significant impact on reanalyzed U_{10} and H_s trends.

It seems at first counterintuitive that the difference between the free-running ERA-20CM and the two reanalyses, ERA-20C and CERA-20C, is greatest in the early period where observations are scarce. The reason is, as Laloyaux et al. (2018) explain (and first noted by Poli et al. 2015), that the observation error for pressure observations in ERA-20C were too small at the start of the century, putting too much weight to the observations located in the subtropical high pressure belt. This generated large positive surface pressure increments over the unobserved Antarctic region. The same effect was found over the Arctic, but not as strongly as in the Southern Hemisphere. To alleviate this, the observation errors were increased in CERA-20C for the early twentieth century and then allowed to decrease with for the more recent, data-rich period (J. Nicolas 2019, personal communication; Laloyaux et al. 2018, their Fig. 11). We note here, however, that there remains a large discrepancy between ERA-20CM and CERA-20C in all locations investigated, both Northern and Southern Hemisphere, and the improvement over ERA-20C is only marginal in terms of surface wind speed (see Fig. 5, third column).

This work found large positive trends for ERA-20C and CERA-20C in areas that correspond to the highest number of observation counts of ICOADS2.5 assimilated data (Fig. 2). Further analysis at four locations around the globe (Fig. 5), shows that the quality of the observations

may be as important as the increasing number of observations in affecting potential spurious trends, especially in the first part of the twentieth century, where the U_{10} and H_s monthly averages significantly differ between reanalyses and the climate model. This is particularly true for the first half of the century (Fig. 5), where the main average differences are found between ERA-20CM and the two reanalyses (ERA-20C and CERA-20C). Since the observations in this part of the century originate only from shipboard observations (Fig. 1), we believe that the quality of the measurements, already questioned in reference studies (Ramage 1987; Peterson and Hasse 1987; Cardone et al. 1990), have a major impact. As a result, it may not be possible to extract reliable trend estimates from reanalysis that extend to the period before 1950.

ERA-20CM seems to perform better than the reanalyses in resolving the spatial distribution of H_s and U_{10} long-term trends. As pointed out by Hersbach et al. (2015a), ERA-20CM outperforms reanalyses such as ERA-20C at large time scales (more than a year) thus being a potential reference model to analyze H_s and U_{10} trends over the last century. Although the ERA-20CM spatial trend distribution proved to be similar to altimeter significant wave height trends, it should be noted that the ERA-20CM realizations, especially in variation in temperature, are closely related to the spread in the HadISST2 ensemble (Hersbach et al. 2015a). That is, the sea surface temperature boundary condition may be a significant contributor to this observed trend. Indeed, we found similarities between ERA-20CM model-only integration and CERA-20C coupled model reanalysis in the yearly average climate for regions such as the Kuroshio Extension area (Fig. 6), where SST-induced winds might explain the effect of the SST boundary conditions on H_s and U_{10} in the reanalyses. The North Pacific, the North Atlantic, the Tasman Sea, and the South Atlantic coasts of Africa and South America are regions characterized by large discrepancies between model and reanalyses trends (Fig. 3), suggesting a significant impact of assimilated ICOADS observations (Figs. 2a,b) on long-term climate analysis of these areas.

The 1985–2010 comparison with satellite altimeter trends further investigated the ECMWF datasets ability in representing long-term climate variations in H_s and U_{10}. The comparison confirmed the superior quality of the ERA-20CM model-only integration in describing the spatial distribution of H_s trends compared to CERA-20C. The CERA-20C H_s trends found in the Southern Hemisphere midlatitudes are somewhat confusing. Model, reanalyses, and satellite altimeter observations agree on a general increase of U_{10} over the Southern Hemisphere in the last part of the twentieth century. However, only the satellite trend results are consistently statistically significant, whereas ERA-20CM and CERA-20C are only sparsely statistically significant at the SKTT 95% level.

Both model and satellite wind and wave time series have limitations. However, these are invaluable tools to understand the global wind-wave climate, and it is fundamental to continue to compare and analyze independent observational and model datasets. It is not possible to identify a general best performing dataset to estimate wind-wave climate trends. However, we might argue that the absence of data assimilation in ERA-20CM, and the larger time span, if compared to the satellite observations, makes this model the more suitable for the analysis of century-long trends. Furthermore, knowledge of the performance and structure of these datasets, may provide insight as to the most appropriate model results for particular areas of the oceans or for a specific time period. Also, these tools may benefit practical applications if their limitations with respect to trend estimates are understood.

The contrasting H_s and U_{10} trend results found in this study, show that the connection between the wind and wave climate trends is not as straightforward as one might think. The model wave height trends may significantly differ from the wind speed trend estimates. Future wind and wave climate trend studies should consider this aspect of the global models.

7. Conclusions

Twentieth-century reanalyses show spurious trends in 10-m surface wind speed U_{10} and significant wave height H_s throughout the whole 1901–2010 period. The increasing number of observations, as well as changes in the quality of the data ingested in these reanalyses, mainly affect four areas of the oceans where H_s and U_{10} trend analyses show the largest discrepancies between the model-only integration and the reanalyses. These are the North Atlantic, the North Pacific, the Tasman Sea, and the South Atlantic region east of South America. The comparison with satellite altimeter trends showed agreement on a general increase of Southern Hemisphere U_{10}. Considerable care must be exercised when considering the assimilation of surface wind measurements before the 1950s. A comparison with the newly available ERA-5 (from 1950 until the present) may further help to detect data assimilation impacts and investigate the nature of H_s and U_{10} climate trend estimates from state-of-the-art reanalyses.

Acknowledgments. IRY wishes to acknowledge the support of the Integrated Marine Observing System (IMOS) in compiling and archiving the altimeter dataset. ØB and OJA gratefully acknowledge the support from EU programme ERA4CS through the WINDSURFER

project and the Research Council of Norway through the ExWaMar project (Grant 256466).

REFERENCES

Aarnes, O. J., S. Abdalla, J.-R. Bidlot, and Ø. Breivik, 2015: Marine wind and wave height trends at different ERA-Interim forecast ranges. *J. Climate*, **28**, 819–837, https://doi.org/10.1175/JCLI-D-14-00470.1.

Allan, J., and P. Komar, 2000: Are ocean wave heights increasing in the eastern North Pacific? *Eos, Trans. Amer. Geophys. Union*, **81**, 561–567, https://doi.org/10.1029/EO081i047p00561-01.

Befort, D. J., S. Wild, T. Kruschke, U. Ulbrich, and G. C. Leckebusch, 2016: Different long-term trends of extra-tropical cyclones and windstorms in ERA-20C and NOAA-20CR reanalyses. *Atmos. Sci. Lett.*, **17**, 586–595, https://doi.org/10.1002/asl.694.

Bengtsson, L., S. Hagemann, and K. I. Hodges, 2004: Can climate trends be calculated from reanalysis data? *J. Geophys. Res.*, **109**, D11111, https://doi.org/10.1029/2004JD004536.

Bertin, X., E. Prouteau, and C. Letetrel, 2013: A significant increase in wave height in the North Atlantic Ocean over the 20th century. *Global Planet. Change*, **106**, 77–83, https://doi.org/10.1016/j.gloplacha.2013.03.009.

Bitner-Gregersen, E. M., and Coauthors, 2018: Climate change and safe design of ship structures. *Ocean Eng.*, **149**, 226–237, https://doi.org/10.1016/j.oceaneng.2017.12.023.

Breivik, Ø., A. Carrasco, J. Staneva, A. Behrens, A. Semedo, J.-R. Bidlot, and O. J. Aarnes, 2019: Global Stokes drift climate under the RCP8.5 scenario. *J. Climate*, **32**, 1677–1691, https://doi.org/10.1175/JCLI-D-18-0435.1.

Buizza, R., and Coauthors, 2018: The EU-FP7 ERA-CLIM2 project contribution to advancing science and production of Earth system climate reanalyses. *Bull. Amer. Meteor. Soc.*, **99**, 1003–1014, https://doi.org/10.1175/BAMS-D-17-0199.1.

Cardone, V. J., J. G. Greenwood, and M. A. Cane, 1990: On trends in historical marine wind data. *J. Climate*, **3**, 113–127, https://doi.org/10.1175/1520-0442003<0113:OTIHMW>2.0.CO;2.

Compo, G. P., J. S. Whitaker, and P. D. Sardeshmukh, 2006: Feasibility of a 100-year reanalysis using only surface pressure data. *Bull. Amer. Meteor. Soc.*, **87**, 175–190, https://doi.org/10.1175/BAMS-87-2-175.

——, and Coauthors, 2011: The Twentieth Century Reanalysis Project. *Quart. J. Roy. Meteor. Soc.*, **137**, 1–28, https://doi.org/10.1002/qj.776.

Cram, T. A., and Coauthors, 2015: The International Surface Pressure Databank version 2. *Geosci. Data J.*, **2**, 31–46, https://doi.org/10.1002/gdj3.25.

de Boisséson, E., M. A. Balmaseda, S. Abdalla, E. Källén, and P. A. E. M. Janssen, 2014: How robust is the recent strengthening of the tropical Pacific trade winds? *Geophys. Res. Lett.*, **41**, 4398–4405, https://doi.org/10.1002/2014GL060257.

Dee, D., M. Balmaseda, G. Balsamo, R. Engelen, A. Simmons, and J.-N. Thépaut, 2014: Toward a consistent reanalysis of the climate system. *Bull. Amer. Meteor. Soc.*, **95**, 1235–1248, https://doi.org/10.1175/BAMS-D-13-00043.1.

Dietz, E. J., and T. J. Killeen, 1981: A nonparametric multivariate test for monotone trend with pharmaceutical applications. *J. Amer. Stat. Assoc.*, **76**, 169–174, https://doi.org/10.1080/01621459.1981.10477624.

Dobrynin, M., J. Murawski, J. Baehr, and T. Ilyina, 2015: Detection and attribution of climate change signal in ocean wind waves. *J. Climate*, **28**, 1578–1591, https://doi.org/10.1175/JCLI-D-13-00664.1.

Gemmrich, J., B. Thomas, and R. Bouchard, 2011: Observational changes and trends in northeast Pacific wave records. *Geophys. Res. Lett.*, **38**, L22601, https://doi.org/10.1029/2011GL049518.

Gower, J., 2002: Temperature, wind and wave climatologies, and trends from marine meteorological buoys in the northeast Pacific. *J. Climate*, **15**, 3709–3718, https://doi.org/10.1175/1520-0442015<3709:TWAWCA>2.0.CO;2.

Gregow, H., and Coauthors, 2016: Worldwide survey of awareness and needs concerning reanalyses and respondents views on climate services. *Bull. Amer. Meteor. Soc.*, **97**, 1461–1473, https://doi.org/10.1175/BAMS-D-14-00271.1.

Gulev, S. K., and V. Grigorieva, 2004: Last century changes in ocean wind wave height from global visual wave data. *Geophys. Res. Lett.*, **31**, L24302, https://doi.org/10.1029/2004GL021040.

——, and ——, 2006: Variability of the winter wind waves and swell in the North Atlantic and North Pacific as revealed by the voluntary observing ship data. *J. Climate*, **19**, 5667–5685, https://doi.org/10.1175/JCLI3936.1.

Hemer, M. A., 2010: Historical trends in Southern Ocean storminess: Long-term variability of extreme wave heights at Cape Sorell, Tasmania. *Geophys. Res. Lett.*, **37**, L18601, https://doi.org/10.1029/2010GL044595.

Hersbach, H., C. Peubey, A. Simmons, P. Berrisford, P. Poli, and D. Dee, 2015a: ERA-20CM: A twentieth-century atmospheric model ensemble. *Quart. J. Roy. Meteor. Soc.*, **141**, 2350–2375, https://doi.org/10.1002/qj.2528.

——, P. Poli, and D. Dee, 2015b: The observation feedback archive for the ICOADS and ISPD data sets. ERA Rep. 18, 31 pp., https://www.ecmwf.int/file/22467/download?token=wFLYGKsZ.

Hirsch, R. M., and J. R. Slack, 1984: A nonparametric trend test for seasonal data with serial dependence. *Water Resour. Res.*, **20**, 727–732, https://doi.org/10.1029/WR020i006p00727.

——, ——, and R. A. Smith, 1982: Techniques of trend analysis for monthly water quality data. *Water Resour. Res.*, **18**, 107–121, https://doi.org/10.1029/WR018i001p00107.

Janssen, P., 2004: *The Interaction of Ocean Waves and Wind*. Cambridge University Press, 300 pp., https://doi.org/10.1017/cbo9780511525018.

Kendall, M. G., 1948: *Rank Correlation Methods*. C. Griffin, 160 pp.

Kent, E. C., D. I. Berry, S. D. Woodruff, and P. K. Taylor, 2006: Voluntary observing ships: A vital marine observing system in decline. *CLIVAR Exchanges*, No. 38, International CLIVAR Project Office, Southampton, United Kingdom, 20–21.

——, and Coauthors, 2019: Observing requirements for long-term climate records at the ocean surface. *Front. Mar. Sci.*, **6**, 441, https://doi.org/10.3389/FMARS.2019.00441.

Kumar, P., S.-K. Min, E. Weller, H. Lee, and X. L. Wang, 2016: Influence of climate variability on extreme ocean surface wave heights assessed from ERA-Interim and ERA-20C. *J. Climate*, **29**, 4031–4046, https://doi.org/10.1175/JCLI-D-15-0580.1.

Laloyaux, P., M. Balmaseda, D. Dee, K. Mogensen, and P. Janssen, 2016: A coupled data assimilation system for climate reanalysis. *Quart. J. Roy. Meteor. Soc.*, **142**, 65–78, https://doi.org/10.1002/qj.2629.

——, and Coauthors, 2018: CERA-20C: A coupled reanalysis of the Twentieth Century. *J. Adv. Model. Earth Syst.*, **10**, 1172–1195, https://doi.org/10.1029/2018MS001273.

Luijendijk, A., G. Hagenaars, R. Ranasinghe, F. Baart, G. Donchyts, and S. Aarninkhof, 2018: The state of the world's beaches. *Sci. Rep.*, **8**, 6641, https://doi.org/10.1038/S41598-018-24630-6.

Mann, H. B., 1945: Nonparametric tests against trend. *Econometrica*, **13**, 245–259, https://doi.org/10.2307/1907187.

Maury, M., 1853: *Maritime Conference Held at Brussels, for Devising a Uniform System of Meteorological Observations at Sea*. Hayez, 125 pp.

Mentaschi, L., M. I. Vousdoukas, J.-F. Pekel, E. Voukouvalas, and L. Feyen, 2018: Global long-term observations of coastal erosion and accretion. *Sci. Rep.*, **8**, 12876, https://doi.org/10.1038/s41598-018-30904-w.

Mogensen, K. S., L. Magnusson, and J.-R. Bidlot, 2017: Tropical cyclone sensitivity to ocean coupling in the ECMWF coupled model. *J. Geophys. Res. Oceans*, **122**, 4392–4412, https://doi.org/10.1002/2017JC012753.

Nonaka, M., and S.-P. Xie, 2003: Covariations of sea surface temperature and wind over the kuroshio and its extension: Evidence for ocean-to-atmosphere feedback. *J. Climate*, **16**, 1404–1413, https://doi.org/10.1175/1520-044216<1404:COSSTA>2.0.CO;2.

Peterson, E., and L. Hasse, 1987: Did the Beaufort scale or the wind climate change? *J. Phys. Oceanogr.*, **17**, 1071–1074, https://doi.org/10.1175/1520-0485017<1071:DTBSOT>2.0.CO;2.

Poli, P., H. Hersbach, P. Berrisford, D. Dee, A. Simmons, and P. Laloyaux, 2015: ERA-20C deterministic. ERA Rep. Series 20, 48 pp., https://www.ecmwf.int/file/23560/download?token=p957150u.

——, and Coauthors, 2016: ERA-20C: An atmospheric reanalysis of the twentieth century. *J. Climate*, **29**, 4083–4097, https://doi.org/10.1175/JCLI-D-15-0556.1.

Ramage, C., 1987: Secular change in reported surface wind speeds over the ocean. *J. Climate Appl. Meteor.*, **26**, 525–528, https://doi.org/10.1175/1520-0450026<0525:SCIRSW>2.0.CO;2.

Ranasinghe, R., 2016: Assessing climate change impacts on open sandy coasts: A review. *Earth Sci. Rev.*, **160**, 320–332, https://doi.org/10.1016/j.earscirev.2016.07.011.

Rayner, N., P. Brohan, D. Parker, C. Folland, J. Kennedy, M. Vanicek, T. Ansell, and S. Tett, 2006: Improved analyses of changes and uncertainties in sea surface temperature measured in situ since the mid-nineteenth century: The HadSST2 dataset. *J. Climate*, **19**, 446–469, https://doi.org/10.1175/JCLI3637.1.

Rhein, M., and Coauthors, 2013: Observations: Ocean. *Climate Change 2013: The Physical Science Basis*, T. F. Stocker et al., Eds., Cambridge University Press, 255–315.

Ribal, A., and I. R. Young, 2019: 33 years of globally calibrated wave height and wind speed data based on altimeter observations. *Sci. Data*, **6**, 77, https://doi.org/10.1038/S41597-019-0083-9.

Ruggiero, P., P. D. Komar, and J. C. Allan, 2010: Increasing wave heights and extreme value projections: The wave climate of the U.S. Pacific Northwest. *Coastal Eng.*, **57**, 539–552, https://doi.org/10.1016/j.coastaleng.2009.12.005.

Sasaki, W., 2016: Impact of satellite data assimilation in atmospheric reanalysis on the marine wind and wave climate. *J. Climate*, **29**, 6351–6361, https://doi.org/10.1175/JCLI-D-16-0056.1.

Semedo, A., K. Sušelj, A. Rutgersson, and A. Sterl, 2011: A global view on the wind sea and swell climate and variability from ERA-40. *J. Climate*, **24**, 1461–1479, https://doi.org/10.1175/2010JCLI3718.1.

Sen, P. K., 1968: Estimates of the regression coefficient based on Kendall's tau. *J. Amer. Stat. Assoc.*, **63**, 1379–1389, https://doi.org/10.1080/01621459.1968.10480934.

Shimura, T., N. Mori, and M. A. Hemer, 2016: Variability and future decreases in winter wave heights in the western North Pacific. *Geophys. Res. Lett.*, **43**, 2716–2722, https://doi.org/10.1002/2016GL067924.

Theil, H., 1950: A rank-invariant method of linear and polynominal regression analysis (parts 1-3). *Ned. Akad. Wet. Proc.*, **53A**, 386–392.

Thomas, B. R., and V. Swail, 2011: Buoy wind inhomogeneities related to averaging method and anemometer type: Application to long time series. *Int. J. Climatol.*, **31**, 1040–1055, https://doi.org/10.1002/joc.2339.

——, E. C. Kent, V. R. Swail, and D. I. Berry, 2008: Trends in ship wind speeds adjusted for observation method and height. *Int. J. Climatol.*, **28**, 747–763, https://doi.org/10.1002/JOC.1570.

Tokinaga, H., and S.-P. Xie, 2011: Wave- and anemometer-based sea surface wind (WASWind) for climate change analysis. *J. Climate*, **24**, 267–285, https://doi.org/10.1175/2010JCLI3789.1.

WAMDI Group, 1988: The WAM model—A third generation ocean wave prediction model. *J. Phys. Oceanogr.*, **18**, 1775–1810, https://doi.org/10.1175/1520-0485018<1775:TWMTGO>2.0.CO;2.

Wang, X. L., and V. R. Swail, 2001: Changes of extreme wave heights in Northern Hemisphere oceans and related atmospheric circulation regimes. *J. Climate*, **14**, 2204–2221, https://doi.org/10.1175/1520-0442014<2204:COEWHI>2.0.CO;2.

——, Y. Feng, and V. Swail, 2012: North Atlantic wave height trends as reconstructed from the 20th century reanalysis. *Geophys. Res. Lett.*, **39**, L18705, https://doi.org/10.1029/2012GL053381.

——, ——, G. Compo, V. Swail, F. Zwiers, R. Allan, and P. Sardeshmukh, 2013: Trends and low frequency variability of extra-tropical cyclone activity in the ensemble of twentieth century reanalysis. *Climate Dyn.*, **40**, 2775–2800, https://doi.org/10.1007/s00382-012-1450-9.

Weisse, R., 2010: *Marine Climate and Climate Change: Storms, Wind Waves and Storm Surges*. Springer Science & Business Media, 219 pp.

Wohland, J., N.-E. Omrani, D. Witthaut, and N. S. Keenlyside, 2019: Inconsistent wind speed trends in current twentieth century reanalyses. *J. Geophys. Res. Atmos.*, **124**, 1931–1940, https://doi.org/10.1029/2018JD030083.

Woodruff, S. D., H. Diaz, J. Elms, and S. Worley, 1998: COADS Release 2 data and metadata enhancements for improvements of marine surface flux fields. *Phys. Chem. Earth*, **23**, 517–526, https://doi.org/10.1016/S0079-194600064-0.

——, and Coauthors, 2011: ICOADS Release 2.5: Extensions and enhancements to the surface marine meteorological archive. *Int. J. Climatol.*, **31**, 951–967, https://doi.org/10.1002/joc.2103.

Young, I. R., 1999a: Seasonal variability of the global ocean wind and wave climate. *Int. J. Climatol.*, **19**, 931–950, https://doi.org/10.1002/(SICI)1097-0088(199907)19:9<931::AID-JOC412>3.0.CO;2-O.

——, 1999b: *Wind Generated Ocean Waves*. Vol. 2, Elsevier, 284 pp.

——, and A. Ribal, 2019: Multiplatform evaluation of global trends in wind speed and wave height. *Science*, **364**, 548–552, https://doi.org/10.1126/science.aav9527.

——, S. Zieger, and A. V. Babanin, 2011: Global trends in wind speed and wave height. *Science*, **332**, 451–455, https://doi.org/10.1126/science.1197219.